PNAS RESEARCH ARTICLE | ENGINEERING

Entanglement-driven responses through multiscale 3D-printed knits

Bradley Cline[a], Catherine Bai[a], Sehui Jeong[b], Ling Xu[c], Yue Wang[a], James U. Surjadi[c], Carlos M. Portela[c], and Tian Chen[a,d,1]

This manuscript was compiled on April 17, 2026

Filamentous entanglements such as textiles achieve resilience and toughness through topology rather than material composition alone. Yet architected materials rarely exploit dense interlooping and sliding contacts to achieve extraordinary physical behavior. While research across mechanics, architecture, and design has linked stitch structure to physical behavior, a predictive quantitative framework has remained elusive. Here we show that knitting can be reinterpreted as a general strategy for designing three-dimensional entangled solids with programmable mechanics. Using a geometrically exact description of each stitch and multi-material 3D-printing — a topology-agnostic fabrication approach — we create planar and volumetric knits whose loop parameters directly control stiffness, strength, and energy dissipation. The printed fabrics faithfully reproduce the nonlinear, anisotropic, and hysteretic responses of conventional machine-knitted textiles. We identify a simple normalization that collapses stress-strain curves across stitch geometries, yarn architectures, constituent materials, and length scales, unifying the behavior of traditional and 3D-printed knits on a single master curve. Extending the topology into the "Z" or stacking direction yields volumetric knits whose stiffness and dissipation can be tuned by imposed pre-strain. Finally, we realize the same architecture from centimeters down to micrometers, culminating in, to our knowledge, the smallest knitted structure ever fabricated. By demonstrating that 3D-printed knits can be interpreted both as a traditional fabric composed of a single yarn and as a novel architected material with defined periodicity, this work establishes entangled filaments as a foundation for a new class of material architectures whose mechanics are encoded in their topology.

Filamentous entanglement | Architected materials | Knit textiles

Significance

Filamentous entanglement underlies the resilience and toughness of systems from polymer networks to textiles, yet most architected materials do not capitalize on this principle. While knitting research across mechanics, architecture, and design has demonstrated that stitch structure governs physical behavior, a quantitative framework linking stitch-level geometry to mechanical response has been lacking. Here we show that 3D printing — as a topology-agnostic fabrication platform — enables systematic exploration of entangled architectures, revealing a simple scaling law that unifies the mechanics of traditional and printed knits across materials, geometries, and length scales, from centimeters down to the smallest knit ever fabricated. This framework yields programmable stiffness and dissipation tunable by topology and pre-strain, establishing entanglement as a design primitive for next-generation metamaterials.

Introduction

For their resilience and toughness, filamentous entanglements emerge ubiquitously in natural and artificial systems across length scales, from polymer-chain- and collagen-networks to forest canopies (1–5). Humans began leveraging entanglement in textiles more than 30,000 years ago, with early evidence of twisting plant fibers, animal sinew, and flax into cords and nets that formed the basis of some of the earliest known flexible structures (6, 7). The industrial revolution transformed textile manufacturing, automating production and enabling rapid, repeatable fabrication of knitted fabrics (8, 9). While modern computerized flatbed machines offer a broad design space encompassing complex stitch patterns and 3D geometries (10, 11), the accessible topologies are ultimately governed by the kinematics of needle beds and yarn carriers (12, 13). Knit designers, when designing knits, consider both physical behavior and knittability in modern knitting machines (10, 11, 14–18). However, the quantitative relationship between stitch-level geometric parameters and the resulting mechanical response remains largely empirical. Yet, fabrics created by interlooping a single contiguous yarn are remarkably resilient and tough: they can undergo large reversible deformations, dissipate energy through frictional sliding, and tough against damage accumulated over repeated use.

Author affiliations: [a]Department of Mechanical and Aerospace Engineering, University of Houston, 4226 Martin Luther King Blvd, Houston, 77002, TX, USA; [b]Department of Mechanical Engineering, Stanford University, 440 Escondido Mall, Stanford, 94305, CA, USA; [c]Department of Mechanical Engineering, Massachusetts Institute of Technology, 77 Massachusetts Ave, Cambridge, 02139, MA, USA; [d]Department of Aeronautics, Imperial College London, Exhibition Rd, London, SW7 2AZ, UK

T.C. conceived this study. B.C., T.C. designed the knit architectures. B.C., C.B., Y.W. fabricated samples, performed mechanical experiments and analyzed data. S.J. conducted DER simulations, L.X., J.U.S., C.M.P. conducted microscopic fabrication and experiments. C.M.P. and T.C. supervised the project. All authors contributed to the manuscript drafting.

There is no competing interests.

[1]To whom correspondence should be addressed. E-mail: tian.chen@imperial.ac.uk

Similar to other highly entangled systems, the topological interactions between the filaments dictate the physical properties alongside the constituent material of the filaments themselves (19–22).

Recent works aim to correlate geometry, friction, and contact mechanics to the anisotropic and hysteretic responses of fabrics (12, 19, 23). With 3D printing, we expose a more fundamental level of programmability. Rather than manipulating a yarn through machine-specific operations, we specify the spatial location and material of the structure on a voxel-by-voxel basis. More broadly, our aim is to explore entangled filamentous material architectures generally – one that encompasses knitting, weaving, chainmail, and beyond. Each existing textile machine is optimized for a particular class of entanglement whereas 3D printing is topology-agnostic. We begin with knitting because well-established industrial benchmarks allow us to validate that printed entanglements faithfully reproduce the mechanics of their conventional counterparts. Works have investigated the mechanical properties of knit textiles in simulation and explored different stitch topologies to tune performance and shape (24, 25). More broadly, knitting research spans disciplines: in architecture, CNC-knitted textiles have been employed as structural formworks for complex concrete shells (26, 27), as force-active building envelopes and sensory-responsive environments (18, 28, 29), and as environmentally responsive programmable material systems (30, 31). These works demonstrate that parametric stitch structure can govern global physical behavior across scales and applications.

In parallel, the field of architected materials has demonstrated how the geometry of the microstructure can be designed to achieve physical behaviors unattainable in homogeneous solids, only recently exploiting the dense entanglement and sliding interactions that define textiles (32–34). Bridging these domains offers a new opportunity: to merge the periodicity and tunability of architected materials with the entanglement and energy dissipation intrinsic to fabrics, yielding a new class of matter whose mechanics arise from both topology and composition. 3D-printing has recently enabled the experimental investigation of interlocking structures such as chainmail, knot and woven assemblies, hinting at broader possibilities for entangled architectures (35–37). Here, we show that knitting can be reimagined as a general strategy for designing three-dimensional entangled material architectures using 3D printing. By formulating a geometrically exact description of each stitch and using 3D-printing, we flexibly create planar and volumetric knits with tunable loop parameters that directly control stiffness, strength, and energy dissipation. Custom machines have been developed to create volumetric knits – notably the solid knitting system of Hirose et al. (38), which achieved interlooping across three axes using a purpose-built apparatus. However, each such machine is tailored to a specific topology, motivating a more flexible fabrication approach for systematic exploration of entangled architectures. These printed knits faithfully reproduce the nonlinear, anisotropic, and hysteretic behavior of conventional fabrics. We uncover a universal scaling law that collapses the stress-strain responses of both traditional and printed knits onto a single master curve, revealing an entanglement-governed relationship independent of material. Extending knitting into three orthogonal directions, we realize volumetric knits with programmable coupling between orthogonal strains and demonstrate that this framework holds across scales by microfabricating knits with loop dimensions on the order of microns. Together, these results establish 3D-printing knits as a new paradigm in architected materials, where programmable mechanical behavior emerges from controlled filament entanglement.

Results

Traditional vs. 3D-printed knits. First, we demonstrate that 3D-printed knits, that is fabrics created with additive manufacturing methods, can faithfully reproduce the mechanical signatures of their conventional counterparts. We therefore examine the construction of planar knitted fabrics — both traditional and 3D-printed — to establish quantitative correspondence and to isolate the role of geometry in governing their response.

We begin by replicating the hierarchical structure of traditional knits from the loop topology to yarn arrangement and fiber count. In the most basic Stockinette (also known as jersey) knit with industrial knitting machines, a homogeneous knit fabric is constructed using a single contiguous yarn (25, 39, 40). Topologically, in basic knits, this yarn is arranged into multiple loops (or stitches) in series to form a row. At the end of a row, the yarn loops to begin the next row in reverse. In this next row, the loops are pulled through the loops in the previous row to create the knit fabric (Fig. 1a). The row and column directions are termed course (C) and wale (W) respectively (Fig. 1a).

To 3D-print knits, we begin by mathematically defining the geometry of each loop. This enables implicit control of the topology of the knit, *i.e.*, the manner in which the yarn loops itself. With such a description, we can directly generate and 3D-print a volumetric representation of a knit using commercial technologies, such as Inkjet 3D-printing (41). The resulting prints replicate the topology, geometry as well as unraveling characteristics of a traditional knit (Fig. 1b). While industrial knitting machines provide a wide range of design space, 3D printing offers a complementary approach: rather than defining geometry through needle operations, we construct the knit voxel by voxel, enabling independent control over loop geometry and constituent material to introduce new architectures. By introducing interlooping in the Z direction, we demonstrate volumetric knit architectures in which a single continuous yarn forms entangled contacts across all three principal axes (Fig. 1c). The unit cell of which features a complex microstructure with multiple seemingly disjointed filaments.

3D-printing knit architecture. In industrial knitting, programming involves specifying low-level operations such as needle movements, yarn carrier motions, and yarn tension, where the final geometry naturally emerges from the physical interactions of interconnected yarn loops and the needles (42–45). In contrast, 3D printing requires the user to explicitly construct a physically feasible mesh prior to fabrication (37). This explicit geometric control enables the systematic parametric sweeps across loop geometry, yarn architecture, and material that underpin the analysis in this work. We begin by defining the centerline of the knit. We then spiral the fiber of the yarn around this

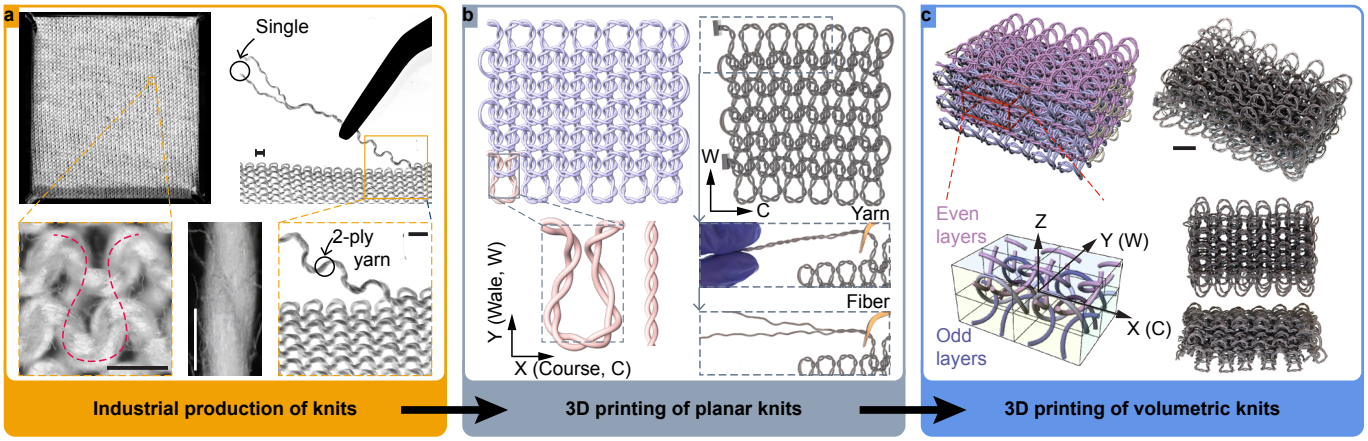

Fig. 1. 3D-printed knit material architectures. **a**, A traditional Stockinette knit with a 2-ply cotton yarn. Unraveling of the knit shows the 2-ply yarn and its constituent singles. The scale bars are 1 mm. **b**, A knit with the same Stockinette topology and 2-ply yarn architecture is 3D-printed using the Polyjet technology. Manual unraveling of the top row shows an individual yarn and its constituent fibers. **c**, A $6 \times 6 \times 6$ volumetric knit showing an additional looping per stitch in the Z direction. A periodic unit consists of many disjointed yarn segments. The scale bar is 10 mm.

centerline (46) (Fig. 2a). As a canonical example, the centerline of a Stockinette stitch $\gamma(t)$ is geometrically described using an arc-length formulation as

$$\gamma(t) = \left[\frac{l}{2\pi}\left(t + a\sin 2t\right), h\cos t, d\cos 2t\right], \qquad [1]$$

where $t \in [0, 2\pi]$ is the arc-length, h, l, a, d are the height, length, curvature and depth of individual loops respectively (46) (See Fig. 2b, and SI for detailed derivations).

We then calculate the Frenet frames around this centerline to define the fiber bundles that spirals around (Fig. 2a). The fiber bundles are parametrized by the distance of separation of the fibers R, tilt angle ω, fiber radius r and count n (Fig. 2b). Curved segments are added between adjacent rows in the Wale direction to maintain contiguity. The same knit and yarn geometry can be seen in a cotton knit of the same topology (Fig. 1a).

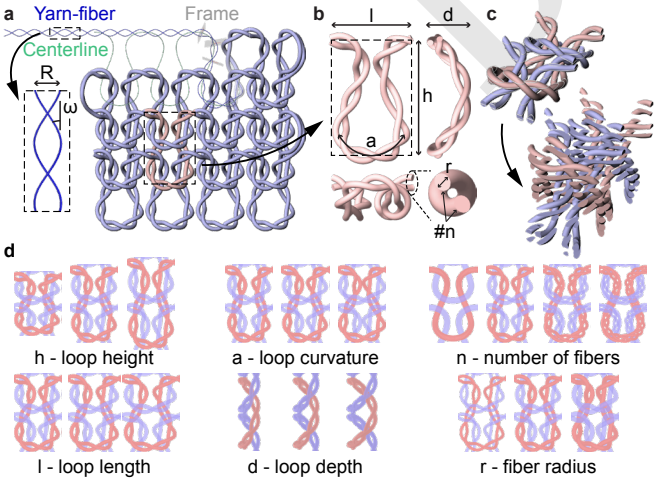

Fig. 2. Design and fabrication of 3D-printed knits. **a**, A centerline is defined, and a yarn-fiber spirals around the centerline based on its Frenet frames. A circular cross-section is assigned to each fiber to create a solid geometry. The yarn-fiber is parameterized by the separation distance and tilt angle. **b**, Parametric design space of the knit fabrics, featuring hierarchical architecture of fibers, yarns, and loop. **c**, Schematic of layer slicing and layer-by-layer 3D-printing using the Polyjet. **d**, Influence of different geometric variables on the shape of the fabric, including loop height, length, depth and curvature, and yarn fiber number and radius.

Using an Inkjet 3D-printing (Stratasys J35), a method where droplets of photopolymer are jetted onto the build platform and then cured with UV lamps to bond layers, we fabricated printed knits from the computational parametrization described above. When the knit is printed in the as-knit configuration, the topological state of entanglement is inherently achieved so long as the triangulated surface mesh contains sufficient clearance such that the yarn does not fuse to itself during printing at crossing points (between loops and between rows). The layer-by-layer deposition along with a water-soluble sacrificial material ensures the fiber bundles remain distinct (Fig. 1c).

To examine the mechanical behavior of such structures, we systematically vary the geometric and material parameters. Specifically, we vary h, l, a, d, n and r which results in different loop geometries (Fig. 2d). Note that when increasing n, the radius r is decreased to maintain total yarn cross sectional area, and to isolate the effect of n. Leveraging multi-material printing, we experiment with two different materials, namely RGD8530-DM (shortened as RGD, $E = 0.82$ GPa) and VeroUltraWhite (shortened as VUW, $E = 2.0$ GPa (47)) (see SI for material behavior).

Mechanics of planar knits. Having shown that 3D-printed knits are geometrically similar to traditional knits, we begin to explore their mechanical behavior. We subject the 3D-printed knits (dimensions L, H) to cyclic equibiaxial strains up to 40% in tension, and measure the reaction force in both the Course and Wale directions, F_C and F_W. Using the overall sample dimensions, we calculate the effective strains and stresses ε_{eff} and σ_{eff} in both directions. Considering that knits are intended to be used as membranes, unit thickness is assumed.

The stress and strain plot of an arbitrarily chosen benchmark specimen exhibits an anisotropic, hystereic, exponential stress-strain behavior (Fig. 3a). Characteristic of knit fabrics, the initial loading exhibits a stiffer response as compared to subsequent loading (25). The unloading curves of each experiment are identical. Similar to "real" fabrics, the Wale direction is stiffer than the

Course, while pronounced hysteresis and dissipation are present. This is due to a combination of stitch dislocation, fiber re-arrangement and frictional contact as well as material viscoelasticity (48).

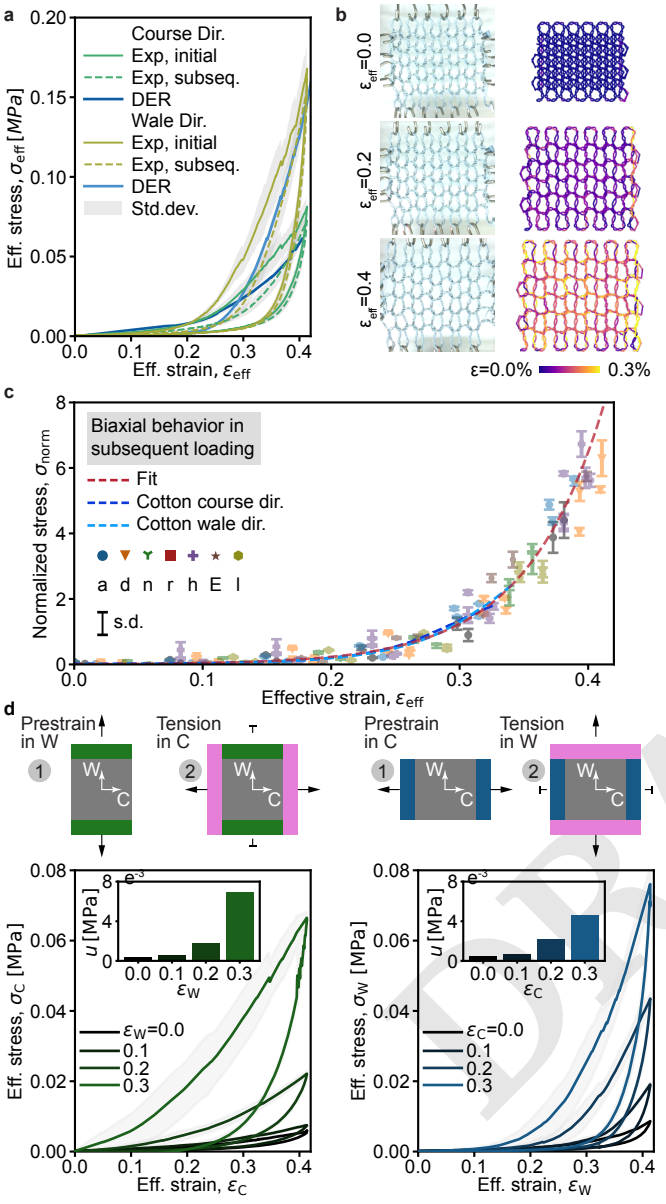

Fig. 3. Mechanical behavior of 3D-printed knits. **a**, Effective stress-strain plot of the knit in both Course (C) and Wale (W) directions of initial and subsequent stretching events. Both anisotropy and hysteresis are observed. **b**, Snapshots of equibiaxial stretching of a 6×6 knit, both in experiments and using Discrete Elastic Rods (DER) simulations. **c**, Normalized stress-strain behaviors of knits printed with different geometric parameters, of a cotton fabric knit using a STOLL system, and of the exponential fit. **d**, Programmable stress-strain behaviors and strain energy dissipation characteristics in Course and Wale directions. In both cases, a pre-strain is imposed in one direction, then the orthogonal direction is loaded and unloaded.

We exploit the fact that we have a complete geometric description of the knit to perform numerical simulations. Computation using volumetric finite elements remains expensive due to the complex frictional contact and sliding that occurs (25). Instead, a Discrete Elastic Rods (DER) based model is adopted (49–51). The Incremental Potential Contact (IPC) toolkit is implemented for contact handling (52–54). In addition to normal contact, tangential sliding is significant in knits where every stitch interacts with neighboring stitches. Therefore, Columbic tangential friction is introduced. The model is tuned to predict subsequent loading events for practicality (Fig. 3b). In addition the global stress-strain behavior, the DER model allows the visualization of yarn-level strain. As the global strain increases biaxially, the curved loops first come into contact with neighboring loops, they then bend to accommodate the tension. At larger strains, since the same yarn travels across the entire fabric, each loops becomes rectangular and axial strain increases. This is distinctively different from uniaxial stretch experiments, where the orthogonal direction contracts to provide slack and the overall arc-length remains unchanged (55, 56).

With the parametric sweep, we observe that the width l and the height h normalize the measured force and displacement to an effective stress σ_{eff} and strain ε_{eff}. An increase in loop depth d and loop curvature a, however, decrease the knit stiffness even as its areal density is increased. Conversely, increasing n and r result in stiffer behavior (see SI for the behavior of individual parametric variations). With these observations, we propose a dimensionless normalization factor,

$$\xi = v\frac{d^3a^2}{E^2n^2r^4} \qquad [2]$$

to derive a normalized stress measure $\sigma_{\text{norm}} = \xi\sigma_{\text{eff}}$ (Eq. 2) that accurately collapses the behaviors to a master curve (Fig. 3c). In ξ, in addition to the geometric parameters shown in Fig. 2d, v accounts for the direction of loading with $v_C = 0.5$ and $v_W = 1.0$, and E is the Young's Modulus of the print materials. This scaling follows from approximating each loop as a curved elastic segment whose bending and contact compliance scale as d^3a^2, while axial stiffness grows with the total yarn second moment of area nr^4.

Using the same normalization with the biaxial behavior of a fabric (Stockinette, cotton) knit using an industrial knitting machine (Stoll CMS), we arrive at the same collapsed behavior, demonstrating that the mechanical behavior of machine-fabricated knits are qualitatively similar to the 3D-printed counterparts (Fig. 3c).

We further propose an empirical relationship to map the effective strain to stress, $\sigma_{\text{eff}} = \alpha e^{\beta\varepsilon_{\text{eff}}}$. Where $\alpha = 900$ and the empirical coefficient $\beta = 16.50$ quantifies the exponential stiffening arising from loop alignment and the progressive engagement of frictional contacts. With this, we are able to directly predict the stress-strain behavior of a knit under arbitrary geometric parameterizations.

Programmable behavior of knits. The fact that 3D-printed knits are all composed of a single yarn hints there exist coupled interactions between the orthogonal stretches of the fabric. We leverage this to demonstrate programmable mechanical behavior. Specifically, we seek to tune the stress-strain relationship in one direction by imposing a pre-strain in the other directions.

We first impose a variable strain between 0.0 to 0.4 in either the Course or the Wale direction. Then we apply a prescribed strain in the other direction up to 0.4. The results show that we can predictably tune the stress output in both Course and Wale directions (Fig. 3d). More pre-stretch in one of the directions increases both the stiffness and the strength of the orthogonal direction. Further, as the specimens recover to the initial position when

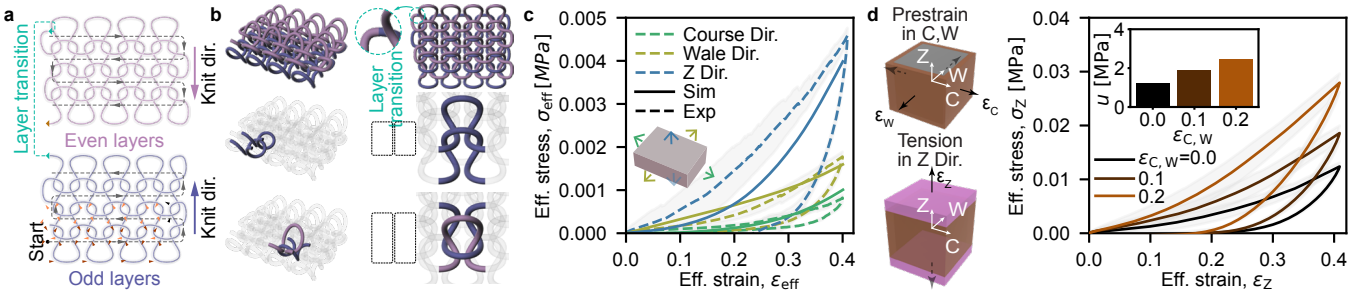

Fig. 4. 3D-printed volumetric knits a, Topology of a volumetric stockinette pattern where even layers are knit in the opposite direction as the odd layers. **b**, When layered in the Z (stacking) direction, a 4×4×2 geometry is formed from a single continuous centerline. The fibers then spiral around this centerline to form the knit. Two distinct loops are present, the first interlaces neighboring rows in the Wale (Y) direction, the second is introduced to interlace neighboring layers in the Z direction. **c**, Uniaxial stretch of a 6×6×6 knit in the three directions exhibit pronounced anisotropic and hysteresis. **d**, Programmable response in the Z direction through equibiaxial strains imposed in both Course (X) and Wale (Y) directions.

unloaded, the hysteric behavior is repeatable and tunable with a larger pre-stretch leading to a larger hysteresis.

The increase of Wale direction pre-strain increases the Course direction secant stiffness up to 0.4% by an order of magnitude from 0.015 to 0.166 MPa. Conversely, the pre-strain in the Course direction increases the Wale direction stiffness from 0.021 to 0.190 MPa. Correspondingly, the dissipated energy density increases from 0.39×10^{-3} to 6.9×10^{-3} MPa and from 0.43×10^{-3} to 4.6×10^{-3} MPa for the Course and Wale direction loading respectively, both representing an increase of over an order of magnitude. Consequently, such knits can be used as a damper to dissipate energy in a tunable manner.

Entanglement towards volumetric knits. We propose the design of a volumetric knit to showcase the ability for 3D-printing to fabricate arbitrary filamentous entanglement. To form a volumetric knit, we introduce the Z direction that is orthogonal to both the Course and Wale directions. On odd-numbered layers, the yarn traverses the fabric in the same manner as the planar knits. It loops from one end to the other on the odd rows, before doubling back on the even rows. Once the entire layer is knit, the yarn travels in the Z direction to arrive at an even-numbered layer, where the knitting direction is reversed (Fig. 4a).

In addition to the looping between neighboring rows, the trigonometry of the centerline formulation is modified to introduce a second form of interlooping that occurs between neighboring layers (38)(Fig. 4b). Specifically, the loops are much taller such that they can loop with the loops above itself. An additional layer transition loop is introduced in between every layer to connect the ends from one layer to the next. These changes are applied to the parameterization of the centerline, from which the fibers are computed through a new set of Frenet frames. The derivations are detailed in the SI.

With these small geometric changes, previously separated knit layers become topologically entangled during printing, yet the knit still maintains the contiguity of a single yarn. This knit structure can be interpreted as an architected material formed by periodically tessellation a single unit cell (Fig. 1c) even through the boundary planes of the unit cell feature disjointed filaments. As such, we conduct uniaxial tension experiments in all three directions. The results show anisotropy with the Z direction being the stiffest (Fig. 4c). As a multi-layered knit, however, the equibiaxial experiments along the Course and Wale directions show similar behavior as in the 2D case (See SI). Numerical modeling of the entire volumetric knit structure using DER accurately predicts the loading path of the stress-strain behavior (Fig. 4c).

Programmable mechanical behavior in the Z direction is achieved by imposing pre-strains in both Course and Wale directions equi-biaxially. A custom triaxial loading frame composed of a biaxial and a uniaxial system is used to experimentally demonstrate the programmability. Equi-biaxial strains of up to 0.2 are imposed. The Z direction is then tensioned until a strain of 0.4. The results show that the effective stiffness as well as the dissipated energy (area between the loading and unloading curves) in Z direction can be programmed (Fig. 4d).

Microscopic knit architecture. To demonstrate the scale invariance of our design framework, we fabricate the same volumetric knit geometry at the micrometre scale using two-photon lithography (Nanoscribe GT2) with a loop size of approximately 50 µm. The structures are printed in IP-Dip photoresist ($E = 3.0$ GPa), with the top and bottom layers fused to load plates to facilitate mechanical testing at the micro-scale. Uniaxial tension experiments are performed *in situ* in the Z direction inside a scanning electron microscope, using a silicon microgripper coupled to a displacement-controlled nanoindenter (Alemnis AG, see Methods) (57).

We then compared the response of the microscale structures with their macroscale counterparts printed with the Inkjet process. The results exhibit comparable deformation sequence at both scales (Fig. 5a). By normalizing the stress response with respect to the material stiffness, the resulting behavior between the macro and the micro experiments are qualitatively similar. The initial stiffening in the micro-scale knit structure can be attributed to localized fusing between fibers. At a strain of approximately 1, these fusing points rupture and the remaining loading curve up to the ultimate strength follows a similar stiffness as the macroscale structure, and both reach approximately the same normalized ultimate tensile strength. While the brittle failure of the macroscale specimen can be attributed to the brittle nature of the Inkjet constituent material, the similarities confirm that the governing mechanism-entanglement-mediated load transfer – is geometric rather than material. Further, this correspondence across four orders of magnitude in length demonstrates that the geometry and physics of

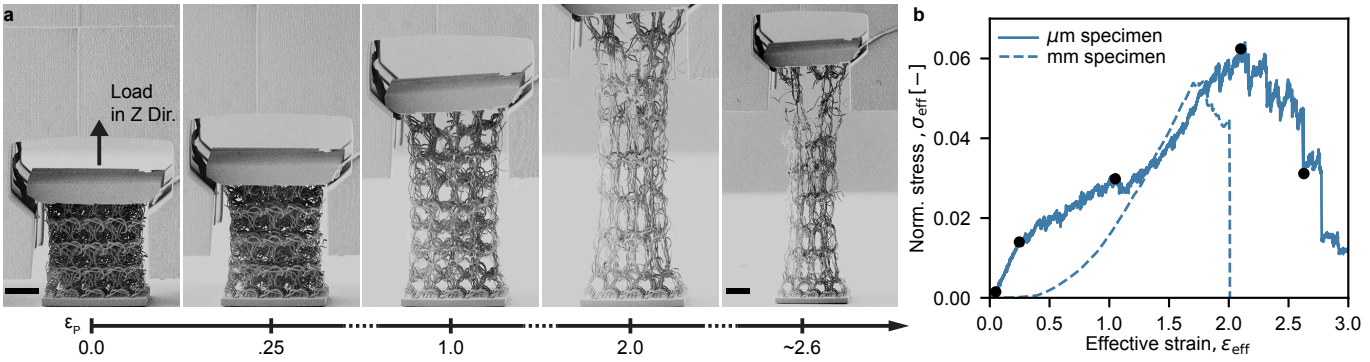

Fig. 5. Uniaxial tension of a microscopic volumetric knit. a, A volumetric knit consisting of 6 loop stitches in each of the X, Y and Z directions printed using the nanoscribe GT2. The scale bar is $50\,\mu m$. **b**, Uniaxial tension experiments comparing the microscopic volumetric knit verses one shown in Fig. 1c up to rupture.

knitted architectures can be applied to tangible fabrics as well as, to our knowledge, the smallest knit ever fabricated.

Discussion

We have shown that 3D-printing can successfully replicate both the geometry and mechanical behavior of traditional knit fabrics, and extend this framework to entangled architectures beyond conventional knitting. By proposing knitting as a strategy for designing entangled architectures, rather than as a fixed textile process, we introduce volumetric knits in which stitches extend and interloop across all three principal axes. These structures behave as periodic entangled solids whose mechanics arise from loop topology, filament geometry, and contact interactions, rather than solely from the base material behavior.

A key outcome of this work is the identification of a simple normalization that collapses the stress-strain responses of different knits onto a single master curve. This collapse, together with the exponential stress-strain relation, suggests that entanglement-mediated load transfer can be captured by a small set of parameters. The same normalization successfully describes both conventional machine-knitted fabrics and their 3D-printed counterparts, indicating that the characteristic nonlinear, hysteretic response of knits is fundamentally geometric and topological.

The programmable behavior we demonstrate emerges directly from the fact that the knits are formed from a single contiguous filament. Pre-strain in one direction reconfigures the network of contacts and slack distribution in the remaining directions, thereby tuning both stiffness and dissipation without altering the underlying architecture. This offers a route to metamaterials whose physical response can be reprogrammed in situ by mechanical conditioning alone. Practically, this tunability can be exploited in reusable impact mitigators, adaptive damping layers, or morphable reinforcements where the same physical device must operate across multiple dissimilar loading regimes.

Our results demonstrate that the geometry and physics of knitted architectures can be meaningfully adapted from tangible fabrics to micrometer-scale structures, culminating in, to our knowledge, the smallest knit ever fabricated. This multiscale continuity suggests that entanglement-based design could be extended toward nanoscale fibers for applications in tissue scaffolding, filtration, and multifunctional composites, as well as towards larger-scale deployable structures or reconfigurable robotics (58). By treating interlooped filaments as a unifying motif across these regimes, this work establishes a foundation for a new class of metamaterial architectures in which resilience, toughness, and programmability are encoded directly in their entangled topology.

Materials and Methods

Methods

Fabrication and characterization of large-scale specimens. The large-scale specimens studied in this manuscript are fabricated using the multi-material Polyjet technology (Stratasys J35). WSS150 is used as the water soluble sacrificial support material. All specimens are soaked in water for a period of 24 hours followed by a drying cycle of 24 hours prior to mechanical testing. The constituent material behavior is discussed in the SI.

Biaxial experiments are conducted using a custom stage described in detail in (25). Each boundary loop is connected with two S-shaped hooks that slide on a metal pole. This enforces displacement in one direction while allowing nearly friction free sliding in the other. Uniaxial experiments use similar clamp setup in conjunction with a commercial testing machine (Instron 68SC-2). Triaxial tensile loading is accomplished by bringing the biaxial stage onto the uniaxial testing setup. All experiments are performed at a displacement speed of $0.2\,mm\,s^{-1}$.

Fabrication and characterization of microscopic specimens. All specimens are manufactured on silicon (Si) substrates using IP-Dip, an acrylate-based photoresist, via two-photon polymerization with a Photonic Professional GT2 system (Nanoscribe GmbH) using the 63x objective. A laser power of $32.5\,mW$ and a scan speed of $10\,mm\,s^{-1}$ are used for the knitted portion, while a laser power of $25\,mW$ and a scan speed of $10\,mm\,s^{-1}$ are used for the monolithic portion (that is, the tensile fixture atop the volumetric knit) to mitigate cavitation. A hatching and slicing distance of $0.2\,\mu m$ are used to fabricate the specimens. After printing, the samples are immersed in propylene glycol monomethyl ether acetate to remove uncured resin for approximately 5 hours. This is followed by a 10-minute rinse in isopropanol. The specimens are then dried using a critical point dryer (Autosamdri 931, Tousimis). Subsequently, the support structures are removed via plasma ashing in air for 30 minutes at $100\,W$. Finally, a 10-nanometer gold coating is applied via sputter coating (SCD 040, Balzers) to enable proper imaging during in situ mechanical tests.

To facilitate real-time observation of the deformation, uniaxial tension tests are performed inside an SEM (Gemini 450, ZEISS) using a custom tensile gripper attached to a nanoindenter (Alemnis AG). The gripper is operated in displacement-controlled mode, with the specimens subjected to a strain rate of approximately $0.001\,s^{-1}$. Stress-strain data are obtained by normalizing the load-displacement measurements with the nominal cross-sectional area and the specimen height, respectively.

Numerical modeling using Discrete Elastic Rods. A combination of Discrete Elastic Rods (DER) and the Incremental Potential Contact (IPC) toolkit is implemented for the simulation, developed based on the ElasticKnots model (54). DER uses principles from Kirchhoff's theory and differential geometry to efficiently calculate the energy and equations of

motion for flexible rods, and IPC acts as a customized nonlinear solver for efficient contact models (49, 52, 53). While only normal contact force is considered for elastic knots, tangential force is significant in knitted structures where every stitch experiences frictional sliding with neighboring stitches. The tangential friction becomes significant with large strain, where the stitches interlock with each other with strong normal repulsion. Thus, we added the tangential friction component. We used the Coulomb friction model, where the friction force is proportional to the normal force and the direction of velocity. We introduced a friction coefficient that determines the magnitude of the friction force. Details are outlined in the SI.

Data, Materials, and Software Availability. The data that support the findings of this study are available in a GitHub repository at https://github.com/UH-AIM/3D-Printing-Volumetric-Knits.

ACKNOWLEDGMENTS. The authors wish to thank P. Liu for her preliminary work on the biaxial testing stage and the Charm Lab at Stanford University (Dr. Okamura and Dr. du Pasquier) for insightful discussions. B.C., C.B., Y.W. and T.C. is partially funded by NASA MIRO "Inflatable Deployable Environments and Adaptive Space Systems" (IDEAS2) Center under Grant no. 80NSSC24M0178.

1. F Burla, Y Mulla, BE Vos, A Aufderhorst-Roberts, GH Koenderink, From mechanical resilience to active material properties in biopolymer networks. *Nat. Rev. Phys.* **1**, 249–263 (2019).
2. S Wu, Chain structure and entanglement. *J. Polym. Sci. Part B: Polym. Phys.* **27**, 723–741 (1989).
3. KA Jansen, et al., The role of network architecture in collagen mechanics. *Biophys. journal* **114**, 2665–2678 (2018).
4. R Seymour, M Tegner, P Dayton, P Parnell, Storm wave induced mortality of giant kelp, macrocystis pyrifera, in southern california. *Estuarine, Coast. Shelf Sci.* **28**, 277–292 (1989).
5. Y Zhang, N Li, G Yang, W Ru, Dynamic analysis of the deployment for mesh reflector deployable antennas with the cable-net structure. *Acta astronautica* **131**, 182–189 (2017).
6. JM Adovasio, O Soffer, B Klíma, Upper palaeolithic fibre technology: interlaced woven finds from pavlov i, czech republic, c. 26,000 years ago. *Antiquity* **70**, 526–534 (1996).
7. O Soffer, JM Adovasio, DC Hyland, The "venus" figurines: textiles, basketry, gender, and status in the upper paleolithic. *Curr. Anthropol.* **41**, 511–537 (2000).
8. P Earnshaw, *Lace machines and machine laces.* (Gorse Publications), (1986).
9. H Liu, H Gong, P Xu, X Ding, X Wu, The mechanism of wrinkling of cotton fabric in a front-loading washer: The effect of mechanical action. *Textile Res. J.* **89**, 3802–3810 (2019).
10. J Underwood, "The design of 3D shape knitted preforms," Doctoral dissertation, RMIT University (2009).
11. DJ Spencer, *Knitting technology: a comprehensive handbook and practical guide.* (CRC Press, Boca Raton, FL) Vol. 16, 1 edition, (2001).
12. X Ding, V Sanchez, K Bertoldi, CH Rycroft, Unravelling the mechanics of knitted fabrics through hierarchical geometric representation. *Proc. Royal Soc. A: Math. Phys. Eng. Sci.* **480** (2024).
13. K Tajiri, R Murakami, S Kobayashi, R Tarumi, TG Sano, Curling morphology of knitted fabrics: Structure and mechanics. *Extrem. Mech. Lett.* **76**, 102300 (2025).
14. V Narayanan, L Albaugh, J Hodgins, S Coros, J McCann, Automatic machine knitting of 3d meshes. *ACM Transactions on Graph. (TOG)* **37**, 1–15 (2018).
15. L Albaugh, J McCann, SE Hudson, L Yao, Engineering multifunctional spacer fabrics through machine knitting in *Proceedings of the 2021 CHI Conference on Human Factors in Computing Systems*, CHI '21. (ACM, Yokohama, Japan), pp. 1–12 (2021).
16. A Zhu, Y Mei, BT Jones, Z Tatlock, A Schulz, Computational illusion knitting. *ACM Transactions on Graph. (TOG)* **43**, 1–13 (2024).
17. M Popescu, M Rippmann, T Van Mele, P Block, Automated generation of knit patterns for non-developable surfaces in *Humanizing Digital Reality*, eds. K De Rycke, et al. (Springer, Singapore), pp. 25–37 (2018).
18. S Ahlquist, Sensory material architectures: Concepts and methodologies for spatial tectonics and tactile responsivity in knitted textile hybrid structures. *Int. J. Archit. Comput.* **14**, 63–82 (2016).
19. SE Gonzalez, MS Dimitriyev, AP Cachine, EA Matsumoto, Pulling apart the mechanisms that lead to jammed knitted fabrics. *Phys. Rev. E* **112**, 015504 (2025).
20. X Chen, LW Taylor, LJ Tsai, An overview on fabrication of three-dimensional woven textile preforms for composites. *Textile Res. J.* **81**, 932–944 (2011).
21. D Roylance, SS Wang, *Penetration mechanics of textile structures.* (Citeseer), (1979).
22. J Engel, C Liu, Creation of a metallic micromachined chain mail fabric. *J. Micromechanics Microengineering* **17**, 551 (2007).
23. K Mahadevan, MC Yuen, V Sanchez, RJ Wood, K Bertoldi, Knitting multistability. *arXiv preprint arXiv:2410.14810* (2024).
24. C du Pasquier, , et al., Haptiknit: Distributed stiffness knitting for wearable haptics. *Sci. Robotics* **9**, eado3887 (2024).
25. C du Pasquier, et al., Multi-level mechanical modeling and computational design framework for weft knitted fabrics. *Extrem. Mech. Lett.* p. 102423 (2025).
26. M Popescu, et al., Building in concrete with an ultra-lightweight knitted stay-in-place formwork: Prototype of a concrete shell bridge. *Structures* **14**, 322–332 (2018).
27. M Popescu, et al., Structural design, digital fabrication and construction of the cable-net and knitted formwork of the KnitCandela concrete shell. *Structures* **31**, 1287–1299 (2021).
28. S Ahlquist, Physical and numerical prototyping for integrated bending- and form-active textile hybrid structures in *Proceedings of the 35th Annual Conference of the Association for Computer Aided Design in Architecture (ACADIA).* (Cincinnati), pp. 143–155 (2015).
29. JE Sabin, D Pranger, C Binkley, K Strobel, J Liu, Lumen in *38th Annual Conference of the Association for Computer Aided Design in Architecture: Recalibration on Imprecision and Infidelity, ACADIA 2018.* (ACADIA), pp. 444–455 (2018).
30. J Scott, Responsive knit: the evolution of a programmable material system. (2018).
31. S McKinlay, S Tibbits, Visualization of three-dimensional knit textiles. (ACADIA), (2023).
32. WP Moestopo, AJ Mateos, RM Fuller, JR Greer, CM Portela, Pushing and pulling on ropes: hierarchical woven materials. *Adv. Sci.* **7**, 2001271 (2020).
33. M Carton, JU Surjadi, BFG Aymon, L Xu, CM Portela, Design framework for programmable three-dimensional woven metamaterials. *Nat. Commun.* **17**, 1581 (2026).
34. E Pescialli, A Munoz Lopez, K Karapiperis, DM Kochmann, Topology-informed design of intertwined architected materials: Unifying woven, knotted, and closed-chain networks. *Mater. & Des.* **260**, 114974 (2025).
35. W Zhou, et al., 3d polycatenated architected materials. *Science* **387**, 269–277 (2025).
36. WP Moestopo, S Shaker, W Deng, JR Greer, Knots are not for naught: Design, properties, and topology of hierarchical intertwined microarchitected materials. *Sci. Adv.* **9**, eade6725 (2023).
37. M Wirth, K Shea, T Chen, 3d-printing textiles: multi-stage mechanical characterization of additively manufactured biaxial weaves. *Mater. & Des.* **225**, 111449 (2023).
38. Y Hirose, M Gillespie, AM Bonilla Fominaya, J McCann, Solid knitting. *ACM Trans. Graph.* **43** (2024).
39. R Granberry, K Eschen, B Holschuh, J Abel, Functionally graded knitted actuators with niti-based shape memory alloys for topographically self-fitting wearables. *Adv. Mater. Technol.* **4**, 1900548 (2019).
40. R Granberry, J Barry, B Holschuh, J Abel, Kinetically tunable, active auxetic, and variable recruitment active textiles from hierarchical assemblies. *Adv. Mater. Technol.* **6**, 2000825 (2021).
41. S Ltd., *Stratasys J35™ Pro PolyJet 3D Printer*, (2023) Technical specifications, build volume, materials, accuracy, etc.
42. M Hofmann, et al., Knitpicking textures: Programming and modifying complex knitted textures for machine and hand knitting in *Proceedings of the 32nd Annual ACM Symposium on User Interface Software and Technology*, UIST '19. (Association for Computing Machinery, New York, NY, USA), p. 5–16 (2019).
43. V Narayanan, K Wu, C Yuksel, J McCann, Visual knitting machine programming. *ACM Transactions on Graph. (TOG)* **38**, 1–13 (2019).
44. K Singal, et al., Programming mechanics in knitted materials, stitch by stitch. *Nat. Commun.* **15**, 2622 (2024).
45. BK Dejene, AD Gudayu, Exploring the potential of 3D woven and knitted spacer fabrics in technical textiles: A critical review. *J. Ind. Textiles* **54**, 15280837241253614 (2024).
46. K Crane, A simple parametric model of plain-knit yarns (online) (2023).
47. S Ltd., Digital materials data sheet: Digital abs plus (https://www.stratasys.com/siteassets/materials/materials-catalog/polyjet-materials/digital-abs-plus/mss_pj_digitalmaterialsdatasheet_0617a.pdf) (2017) MSS_PJ_DigitalMaterialsDataSheet_0617a, PDF.
48. C Jiang, T Gast, J Teran, Anisotropic elastoplasticity for cloth, knit and hair frictional contact. *ACM Transactions on Graph. (TOG)* **36**, 1–14 (2017).
49. M Bergou, M Wardetzky, S Robinson, B Audoly, E Grinspun, Discrete elastic rods. *ACM Transactions on Graph. (TOG)* pp. 1–12 (2008).
50. C Yuksel, JM Kaldor, DL James, S Marschner, Stitch meshes for modeling knitted clothing with yarn-level detail. *ACM Transactions on Graph. (TOG)* **31**, 1–12 (2012).
51. G Sperl, RM Sánchez-Banderas, M Li, C Wojtan, MA Otaduy, Estimation of yarn-level simulation models for production fabrics. *ACM Transactions on Graph. (TOG)* **41**, 1–15 (2022).
52. M Li, et al., Incremental potential contact: intersection-and inversion-free, large-deformation dynamics. *ACM Trans. Graph.* **39**, 49 (2020).
53. M Li, DM Kaufman, C Jiang, Codimensional incremental potential contact. *arXiv preprint arXiv:2012.04457* (2020).
54. M Vidulis, Y Ren, J Panetta, E Grinspun, M Pauly, Computational exploration of multistable elastic knots. *ACM Transactions on Graph.* **42**, 1–15 (2023).
55. S Poincloux, M Adda-Bedia, F Lechenault, Geometry and elasticity of a knitted fabric. *Phys. Rev. X* **8**, 021075 (2018).
56. J Crassous, S Poincloux, A Steinberger, Metastability of a periodic network of threads: Shapes of a knitted fabric. *Phys. Rev. Lett.* **133**, 248201 (2024).
57. JU Surjadi, BF Aymon, M Carton, CM Portela, Double-network-inspired mechanical metamaterials. *Nat. Mater.* **24**, 945–954 (2025).
58. V Sanchez, et al., 3d knitting for pneumatic soft robotics. *Adv. functional materials* **33**, 2212541 (2023).